Clim. Past Discuss., 11, 3211–3239, 2015
www.clim-past-discuss.net/11/3211/2015/
doi:10.5194/cpd-11-3211-2015

Climate of the Past
Discussions
Open Access

Terrigeneous material supply to the Peruvian central continental shelf (Pisco 14° S) during the last 1100 yr: paleoclimatic implications

F. Briceño Zuluaga[1,2], A. Sifeddine[1,2,3], S. Caquineau[2,3], J. Cardich[1,2], R. Salvatteci[2,3,5], D. Gutierrez[2,4], L. Ortlieb[2,3], F. Velazco[2,4], H. Boucher[2,3], and C. Machado[1,2]

[1]Departamento de Geoquímica, Universidade Federal Fluminense, UFF, Niterói, RJ, Brasil
[2]LMI PALEOTRACES (IRD-France, UPMC-France, UA-Chile, UFF-Brazil, UPCH-Peru), Departamento de Geoquímica – UFF, Niterói, Brazil
[3]IRD-Sorbonne Universités (UPMC, CNRS-MNHN), LOCEAN, IRD France-Nord, Bondy, France
[4]Instituto del Mar del Peru IMARPE, Lima, Perú
[5]Institute of Geoscience, Department of Geology, Kiel University, Germany

Terrigeneous material supply to the Peruvian central continental shelf

F. Briceño Zuluaga et al.

Received: 16 June 2015 – Accepted: 18 June 2015 – Published: 17 July 2015

Correspondence to: F. Briceño Zuluaga (franciscojavier@id.uff.br)

Published by Copernicus Publications on behalf of the European Geosciences Union.

Abstract

In the Eastern Pacific, lithogenic input to the ocean is a response of the atmospheric and ocean system variability and their teleconnections over different timescales. Atmospheric (e.g., wind fields, precipitation), hydrological (e.g., fresh water plumes) and oceanic (e.g., currents) conditions determine the transport mode and the amount of lithogenic material transported from the continent to the continental shelf. Here, we present the grain size distribution of a composite record of two laminated sediment cores retrieved in the Peruvian continental shelf, covering the last ∼ 1100 yr at sub-decadal to centennial time-series resolution. We then discuss the paleo-environmental significance and the climatic mechanisms involved. Four grain size modes were identified. Two are linked to aeolian inputs (M3: 53.0 µm and M4: 90.8 µm on average), the third is interpreted as a marker of sediment discharge (M2: 9.4 µm on average), and the last is without an associated origin (M1: ∼ 3 µm). The coarsest components (M3 and M4) dominated during the Medieval Climate Anomaly (MCA) and Current Warm Period (CWP) periods, suggesting that aeolian transport increased as consequence of wind stress intensification. In contrast, M2 displays an opposite behavior, exhibiting an increase in fluvial terrigenous input during the Little Ice Age (LIA), in response to more humid conditions. Comparison with other South American paleoclimate records indicates that the observed changes are driven by interactions between meridional displacement of the Intertropical convergence zone (ITCZ) and of the South Pacific Sub-tropical High (SPSH) at decadal and centennial time scales.

1 Introduction

Along the Peruvian coast, the Pisco region represents a quite intense upwelling zone. This is due to intense alongshore wind, driving coastal upwelling and ultimately increasing marine productivity. Regional wind can be affected at interannual timescales by El Niño Southern Oscillation (ENSO) variability (i.e., enhanced or weakened during

CPD
11, 3211–3239, 2015

La Niña and El Niño events, respectively), as well as by the Pacific Decadal Oscillation (PDO) at decadal timescales. There are different sources and mechanisms controlling the terrigenous material input to the Peruvian continental shelf. Saukel et al. (2011) found that wind is the major transport agent of terrigenous material into the Peru–Chile Trench, between 5 and 25° S. Flores-Aqueveque et al. (2012) showed that in the arid region of Northern Chile, coarser particle (approximately ∼ 100 µm) transport is directly related to interannual variations in the domain of the strongest winds. The Pisco region is also home to local dust storms called "Paracas", which transport dust material to the continental shelf as a response to seasonal erosion and transport events in the Ica desert (∼ 15° S). This process reflects atmosphere stability conditions and coastal sea surface temperature connections (Gay, 2005). In contrast, sediment fluvial discharge is more important in the North where there are large rivers, decreasing southward where arid conditions are dominant (Garreaud and Falvey, 2009; Scheidegger and Krissek, 1982). This discharged material is redistributed southward by coastal currents along the continental shelf (Montes et al., 2010). In addition, small rivers exist in our study area, such as the Pisco river, which has increased flow during el Niño events (Bekaddour et al., 2014). It has also been demonstrated that during El Nino events and coincident positive PDO, there is an increase in precipitation along Northern Peru and, consequently, higher river discharge, mainly from the big rivers (e.g., the Santa river), whereas an opposite trend is observed during La Niña events and the negative phase of PDO (Bekaddour et al., 2014; Böning and Brumsack, 2004; Lavado Casimiro et al., 2012; Ortlieb, 2000; Rein, 2005, 2007; Scheidegger and Krissek, 1982; Sears, 1954).

Grain size distribution in laminated marine sediments may indicate a mixing of particles from different sources and/or deposition processes, expressed as polymodal distributions (e.g., Pichevin et al., 2005; Saukel et al., 2011; Stuut et al., 2005, 2002; Sun et al., 2002; Weltje and Prins, 2003, 2007). This polymodal distribution makes the classification of grain size composition an essential step in identifying the different grain size classes for reconstructing past environmental conditions (e.g., climate, atmosphere and ocean circulation) (Alfaro et al., 2011; Bloemsma et al., 2012; Flores-

CPD
11, 3211–3239, 2015

Aqueveque et al., 2012, 2015; Pichevin et al., 2005; Ratmeyer et al., 1999; Saukel et al., 2011; Stuut et al., 2005, 2007; Sun et al., 2002). The grain-size distribution of lithogenic material of marine sediments can thus be used to infer relative wind strengths and aridity on the assumption that more vigorous atmospheric circulation will transport coarser particles to a short distance and that the relative abundance of fluvial particles reflects seasonal precipitation excess (e.g., Hesse and McTainsh, 1999; Parkin and Shackleton, 1973; Pichevin et al., 2005; Stuut and Lamy, 2004; Stuut et al., 2002).

A significant number of published papers have described the climatic, hydrologic and oceanographic changes during the last 2000 years in the Eastern Pacific region (Sifeddine et al., 2008; Mann et al., 2009; Gutierrez et al., 2011; Salvatteci et al., 2014; Ehlert et al., 2015). These climatic changes have affected the Humboldt Current circulation system and the precipitation pattern in the South Eastern Pacific in general, especially in the Pisco region. Agnihotri et al. (2008) suggested that the Peruvian Upwelling Ecosystem (PUE) is interspersed by periods of high and low productivity and denitrification, modulated by solar forcing at a centennial time-scale. Salvatteci et al. (2014) interpreted that the Medieval Climatic Anomaly (MCA) exhibits two distinct patterns of PUE characterized by weak/intense marine productivity and sub-surface oxygenation, respectively, as a response to strength variation of the Walker circulation, whereas during the Little Ice Age (LIA), an increased sediment discharge was driven by a southward displacement of the ITCZ (Sifeddine et al., 2008; Gutierrez et al., 2009; Salvatteci et al., 2014). In addition, during the Current Warm Period (CWP), the PUE exhibited (1) an intense Oxygen Minimum Zone (OMZ) and an increase in marine productivity, (2) a significant SST cooling (~ 0.3–$0.4\,^{\circ}\mathrm{C\,decade}^{-1}$), and (3) an increase in terrigenous material input (Gutierrez et al., 2011). Those changes during the last Millennium in the South Eastern Pacific region seem to be linked to regional and local climatic phenomena, which had a significant impact on regional rainfall and local wind stress. Nevertheless, little is known about how the regional and local climatic variability impact sedimentation processes (i.e., Aeolian/Fluvial) in the Pisco region. This study aims to reconstruct the variation of the supply of terrigenous material to the Central Peruvian

CPD
11, 3211–3239, 2015

continental shelf, to determine how regional and local river fresh water discharge and local wind field conditions have affected sedimentary deposition processes in the continental Peruvian shelf region (Pisco region), and to unravel the climatic mechanisms behind these processes during the last ∼ 1100 yr.

2 Materials and methods

The B040506 "B6" (14°07.90′ S, 76°30.10′ W, 299 m water depth) and the G10-GC-01 "G10" (14°22.96′ S, 076°23.89′ W, 313 m water depth) sediment cores were retrieved from the central Peruvian continental shelf in 2004 during the Paleo2 cruise onboard the Peruvian José Olaya Balandra vessel (IMARPE) and in 2007 during the Galathea-3 cruise, respectively (Gutiérrez et al., 2009). Lithological descriptions and chronological models of B6 (covering the last ∼ 700 yr) and G10 (covering from ∼ 900 to 1500) are provided by Sifeddine et al. (2008), Gutiérrez et al. (2009) and Salvatteci et al. (2014), respectively. The G10 core chronological model was discussed by Salvatteci et al. (2014) in detail. For the last century, which is recorded only by B6, the age model was based on downcore natural excess ^{210}Pb and ^{230}Th distributions and supported by bomb-derived ^{241}Am distributions. Beyond the last 130 yr, the age model of the B6 core was inferred by ^{14}C-calibrated AMS age distributions.

The spatial regularity of the initial core sampling combined with the natural variable sedimentation rate implied variable time rates between samples (182 samples in total). To compare grain size component variations all along the cores, a downsampling method was applied. This method had three steps: linear interpolation, running average and sample selection. For each core, the interpolation frequency was chosen as the shortest period between two samples. Then, a central running average was windowed in the largest period encountered within each series. Finally, this largest period was used as the selection rate. The regular selection grid was placed among computed data so that the downsample dates were as close as possible with the initial sample

CPD
11, 3211–3239, 2015

dates. This downsampling method provided data with regular frequencies (subsample) so that the observed variations could not be linked to sampling biases.

2.1 Grain size analyses

To isolate the mineral fraction, organic material, calcium carbonates and biogenic silica were successively removed using H_2O_2 (30 % at 50 °C for 3 to 4 days), HCl (10 % for 12 h) and Na_2CO_3 (1 M at 90 °C for 3 h). Between each chemical treatment, samples were repeatedly washed with deionized water and centrifuged at 4000 rpm until the solution became neutral (pH: 6–7) again. Finally, all samples were passed through a 200 µm mesh before analysis because only particles having equivalent diameters less than 200 µm can be detected by the analytical method used. After pre-treatment, the grain size distribution was determined with an automated image analysis system (model FPIA3000, Malvern Instruments in which FPIA stands for Flow Particle Image Analyzer, ALYSES facilities at IRD, Bondy-France). This system is based on a CCD (Charge Coupled Device) camera that captures images of all of the particles homogeneously suspended in a dispersal solution by rotation (600 rpm) in a measurement cell. After magnification (×10), the images are analyzed automatically and the equivalent spherical diameter (defined as the diameter of the spherical particle having the same surface as the measured particle) is determined. The optical magnification used (×10) implies that only particles with equivalent diameters between 0.5 and 200 µm are counted. It is worth noting that this system gives the size distribution and also displays images of the individual particles. If one ignores the images, this method provides size information comparable to that obtained with a laser granulometer. Nevertheless, the images are very useful to check the efficiency of the pre-treatments, and if necessary, non-mineral particles or aggregated mineral particles can be manually removed from the size distributions. The whole measurement range is divided into 225 equal logarithmical steps. Because the size-bins selected by the manufacturer are quite narrow, the number of particles counted in some of them can be limited to just a few units, in which case the associated relative error can be very large. To reduce error, we decided

CPD
11, 3211–3239, 2015

to divide the number of size-bins by a factor of 5 (we use 45 instead of the 225 original ones) and group the number of particles counted in each class. Grain size distributions are expressed as volume distributions.

2.2 Determining sedimentary components and the de-convolution fitting model

As different sediment transport/deposition processes are known to influence the grain-size distribution of the lithic fraction of sediment material (e.g., Gomes et al., 1990; Holz et al., 2007; Pichevin et al., 2005; Prins et al., 2007; Stuut et al., 2005, 2002; Sun et al., 2002; Weltje and Prins, 2001, 2003, 2007; Weltje, 1997), identifying the individual components of the polymodal grain size distribution is decisive for paleoenvironmental reconstructions. The numerical characteristics (e.g., amplitude *A*, geometric mean diameter Gmd, and geometric standard deviation Gsd) of the individual populations whose combination forms the overall grain size distribution were determined for all analyzed samples using the iterative least-square method of Gomes et al. (1990). This fitting method aims to minimize the difference between the volume of particles counted in each size class and that recomputed from the mathematical expression (based on log-normal functions). The number of individual grain-size populations to be used is determined by the operator, and all statistical parameters (e.g., *A*, Gmd and Gsd) are allowed to change from one sample to another. This presents a strong advantage compared to end-member modeling of Weltje (1997) in which the elementary distributions are maintained constant over the whole time series (the only changing parameter being their relative amplitude). Indeed, it is unlikely that the parameters that govern both transport and deposition of lithogenic sediments, and therefore grain size of particles, remain constant over time. This could lead to variations in statistical parameters (e.g., Gmd and Gsd).

CPD
11, 3211–3239, 2015

3 Results and discussion

3.1 Basis for interpretation

Both sediment cores (B06 and G10) exhibit roughly a bimodal grain-size distribution presenting significant variation in amplitude and width. These modes correspond to fine-grain-size classes from ∼ 3–15 µm and coarser grain-size classes between ∼ 50–120 µm (Fig. S1 in the Supplement). A principal component analysis (PCA) based on Wentworth (1922) grain-size classification identifies four groups that could explain the total variance of the dataset (Fig. S2). The observed and modeled grain-size distributions show high correlations ranging from $R^2 = 0.75$ to 0.90, attesting to the fact that the model can provide reliable interpretations (Fig. 2a). Lower correlations occurred when the lithological material proportion was small compared to silica, organic matter and bulk carbonate (6 samples). This situation is met when the number of lithological particles remaining after the chemical attack of these samples was significantly lower, placing it at the limit of statistical representation. However, these samples were considered to be maintained in the analysis because they all presented a high contribution of the coarser particles. Geometrical standard deviation (Gsd) vs. Geometrical mean diameter (Gmd) was plotted where the four individual grain size populations can be easily distinguished (Fig. 2b). The first case (M1), with a Gmd of approximately 3 ± 1 µm, and the second group (M2), with a Gmd of 10 ± 2 µm, are characterized by larger Gsd with a low degree of sorting. According to Sun et al. (2002), such a low degree of sorting (Gsd $\sim 2\sigma$) suggests a slow and continuous depositional process. The coarse modes of M3 and M4 showed mean Gmd values of 54 ± 11 and 91 ± 11 µm, respectively. These modes presented Gsd values closer to 1σ. This is consistent with the optimal grain size transported under favorable erosional soil properties and low wind friction velocity (Iversen and White, 1982; Shao and Lu, 2000; Marticorena, 2014).

In the vicinity of desert areas, where wind-blown transport prevails, size particles with grain size as high as ∼ 100 µm can accumulate in marine sediments (e.g., Stuut et al., 2007; Flores-Aqueveque et al., 2015). In this area, the emissions and transport of mineral particles are related to strong wind events called "Paracas". Paracas dust emission is a local seasonal phenomenon that occurs in winter (September–November) and is due to an intensification of the local surface winds (Schweigger, 1964; Escobar Baccaro, 1993). The pressure gradient of sea level between 15–20° S, 75° W is the controlling factor of Paracas winds (Quijano, 2013). Additionally, local topography influences Paracas events (Gay, 2005).

These coarse particles cannot have a fluvial origin because substantial hydrodynamic energy is necessary to mobilize particles of this size, and because this region is devoid of large-sized rivers (Scheidegger and Krissek, 1982). Rein et al. (2004), followed by Bekaddour et al. (2014), discussed the influence of the changes in the climatic regime as a control of the intensification and variability in the sedimentation of detrital material of fluvial origin in the region. Thus, the continental shelf off of Pisco receives coarse aeolian particles by saltation and suspension processes linked to Paracas events as well as fluvial particles from the few rivers that reach the coast in this region.

Therefore, the coarser grain populations (M3 and M4) can be interpreted as markers of aeolian transport resulting from surface winds and emission processes (e.g. Paracas events) (Flores-Aqueveque et al., 2015; Hesse and McTainsh, 1999; Marticorena and Bergametti, 1995; McTainsh et al., 1997; Sun et al., 2002). These two components (M3 and M4) indicate a local and proximal source (i.e., Paracas winds). This is in contrast to the Atacama Desert source suggested by Ehlert et al. (2015) and Molina-Cruz, (1977). Ehlert et al. (2015), who used the same sediment core (B6), also indicated difficulties in the interpretation of the detritical Sr isotopic signatures as an indicator of the sources. These difficulties can be associated with the variability of the $^{87}Sr/^{86}Sr$ due to grain size (Meyer et al., 2011). The finest M1 component (~ 3 µm) may be linked to both aeolian and fluvial transport mechanisms, or alternatively, may come from aggregates of other particles. Thus, because its origin is difficult to determine, and because its trend appears as relatively independent from the other components, we do not further use it.

The M2 component (~ 10 µm) is interpreted as characteristic of fluvial transport (Koopman et al., 1981; McCave et al., 1995). The fluvial origin of the M2 component is also demonstrated by its trend along the core, which differs from those of M3 and M4. A fluvial origin of this M2 component is also supported by geochemical proxies by an increase in the Ti content input (Sifeddine et al., 2008; Salvatteci et al., 2014) and radiogenic isotope compositions of detrital components (Ehlert et al., 2015), indicating more terrigenous transport during the LIA, where humid conditions are dominant. This M2 component is interpreted as linked to river material discharge, mostly from the north Peruvian coast, and redistributed by oceanic southward coastal currents (Montes et al., 2010; Scheidegger and Krissek, 1982; Unkel et al., 2007).

3.2 Fluvial and aeolian input variability during the past ~ 1100 yr

Grain size component (M2, M3 and M4; Table 1) variations along the composite records (B6 and G10) express fluvial runoff and aeolian multi-decadal to centennial-scale changes. This variability allowed the identification of three major climate periods: MCA, LIA and CWP. The sediments deposited during the MCA exhibit two contrasting distributions of grain size patterns. In the first sequence, dated from 900 to 1170 AD, low values of $D50$ were found varying around 16 ± 6 µm, and explained by 50 ± 10 % M2, 18 ± 7 % M3, 21 ± 8 % M4 and 11 ± 4 % M1 contributions. A second sequence, dated from 1170 to 1450 AD, was marked by high values of $D50$ in the range of 28 ± 17 µm, with average contributions of 14 ± 6 % for M1 and 41 ± 10 % for M2, and values ranging from 21 ± 9 % for M3 and 24 ± 15 % for M4. These results indicate high variability of transport particles during the MCA, with more sediment discharge from 900 to 1170, and more aeolian material input between 1170 and 1450 AD (Fig. 3a).

During the LIA (1450–1800 AD), the deposited particles were dominated by fine grain sizes with a $D50$ varying around an average of 13 ± 9 µm, explained by 57 ± 13 % M2 contribution. The M3 presented an average contribution of 16 ± 8 % and ranged from 5 to 45 %, whereas M4 showed an average contribution of 11 ± 7 % and varied from 0 to 24 % during the same period. This significant contribution of the finest particles of M2 suggests a high fluvial terrigenous input. It is important to note that M2 contributions increased from the beginning to the end of the LIA at 1800 AD (Fig. 3a), suggesting a gradual increase in sediment discharge input (Fig. 3c). Indeed, during the LIA, our results agree with previous studies (Apaéstegui et al., 2014; Gutiérrez et al., 2009; Salvatteci et al., 2014; Sifeddine et al., 2008), indicating wet conditions over the drainage basins. These results also imply that this period was characterized by weak surface winds.

Finally, $D50$ variations show high variability during the last 250 yr of these two periods (1750 to 1850 and 1900 to 1960 AD within the CWP) characterized by high D50 values varying around 45 µm, with ∼ 40 and ∼ 30 % M4 and M3, respectively. From 1850 to 1900 AD and from 1960 to 2000 AD in the CWP, $D50$ displayed values of approximately 20 µm explained by ∼ 40 % M2. Our results indicate a clear increase in coarse (M3 and M4) aeolian material deposition during the CWP, especially from 1750 to 1850 and 1900 to 1960 AD. Moreover, it is noteworthy that during these two periods, coarser particles as large as ∼ 120 µm (in M4 component) were found, indicating extreme wind events (Fig. 3f). On the contrary, the fluvial sediment discharge was the dominant transport mechanism between 1850 and 1900 AD, as well as between 1960 and 2000 AD. The finest particles exhibit a progressive increase during the last 50 years, suggesting an increase in the terrigenous sediment discharge related with fluvial input. A similar trend was observed in the total terrigenous flux record of Pisco and Callao (Sifeddine et al., 2008).

3.3 Climatic interpretations

Our findings suggest a combination between regional and local atmospheric circulation mechanism changes, which controlled the pattern of sedimentation in the study region. Our record is located under the contemporary seasonal Paracas dust storm path, but it also records discharged fluvial mud, often supplied by the rivers along the Peruvian coast. Hence, this record is particularly well suited for a reconstruction of continental runoff/wind intensity in the central Peruvian continental shelf during the last millennium.

CPD
11, 3211–3239, 2015

The interpretation of the changes in the single records of the components (M2, M3 and M4) and their associations (e.g., ratios) can reflect paleoclimatic variations in response to changes in atmospheric conditions. Here, we used the ratio between the aeolian components, defined as the contribution of the stronger winds over total wind variability: M4/(M3 + M4). We used this ratio as a proxy of the local wind intensity (Fig. 4f). In fact, the use of grain-size fraction ratios as a paleoclimate indicator for atmospheric conditions and circulation has been successfully applied to explain different records (Holz et al., 2007; Huang et al., 2011; Prins, 1999; Shao et al., 2011; Stuut et al., 2002; Sun et al., 2002; Weltje and Prins, 2003).

As explained above, the MCA was characterized by a sinuous peak structure that depicts two different climate stages. A first stage spanning from ∼ 900 to 1170 AD is dominated by a high sediment discharge linked to a precipitation increase. This precipitation increase can be explained by the Southward displacement of the ITCZ and a reduction of the SPSH (weaker favorable upwelling winds) (Fig. 4e). This pattern linked to the reorganization of the atmospheric and ocean circulation is also underlined by Salvatteci et al. (2014) using biogeochemical proxies from an ocean sediment record, showing sub-oxic sediment conditions (demonstrated by high values of the Re/Mo ratio), indicating a weaker OMZ intensity (Fig. 4c) probably associated with El Nino-like conditions. Less fluvial input (i.e., dry conditions) and more intense winds characterized the second stage of the MCA (∼ 1170 to 1350 AD) linked to the intensification of SPSH as a response of a northward ITCZ-SPSH meridional displacement. These latter features are in phase with a period of strong OMZ off of Pisco (Fig. 4c), associated with more intense upwelling conditions from a more intense Walker circulation, reflecting La Niña-like conditions. In agreement with Salvatteci et al. (2014), these patterns are consistent with persistent austral summer-like conditions. The association of the ocean-atmospheric system showed that the MCA underwent rapid and abrupt large atmospheric circulation changes.

Our results combined with other paleo-reconstructions suggest that the LIA exhibited a weakening of the regional atmospheric circulation and winds favorable for upwelling.

CPD
11, 3211–3239, 2015

During the LIA, the mean climate state was controlled by a gradual intensification of the fluvial input to the continental shelf, thus indicating wetter conditions (Fig. 4e). These conditions are confirmed by an increase in the terrigenous sediment flux, as described by Sifeddine et al. (2008) and Gutierrez et al. (2009) (Fig. 4d) and demonstrated by the radiogenic isotopic composition of the terrigenous fraction (Ehlert et al., 2015). This increase in wet conditions is also marked by an intensification of the South American Monsoon System (SAMS). Paleo-precipitation records support these regional characteristics (Apaéstegui et al., 2014; Haug et al., 2001; Peterson and Haug, 2006). These conditions were consistent and suggest a direct relationship with the southern meridional displacement of the ITCZ (Fig. 4b). This feature is accompanied by the prevalence of weak winds and noticeable sub-oxic conditions in the sea surface sediment (Salvatteci et al., 2014) (Fig. 4c). These characteristics also support the hypothesis of the ITCZ-SPSH southern meridional displacement and are consistent with a weakening of the Walker circulation (Fig. 4a).

The transition period between the LIA and CWP appears as an abrupt event showing a progressive positive anomaly in the wind intensity and a strong and rapid decrease in the fluvial input to the continental shelf. This suggests a rapid combination of factors: the meridional factor (ITCZ) and the zonal factor (ENSO), which control the input of terrigenous material. Gutiérrez et al. (2009) found evidence of a large reorganization in the tropical Pacific climate with immediate effects on ocean biogeochemical cycling and ecosystem structure at the transition between the LIA and CWP. The increase in the wind intensity (Fig. 4f) suggests northward displacement of the ITCZ-SPSH system, which increased the regional winds favoring aeolian erosive processes and simultaneously showed an increase in the OMZ intensity (Fig. 4c).

Finally, during the CWP (~ 1900 AD to present), negative anomalies in the trend of fluvial input (Fig. 4e) were combined with an increase in wind intensity (Fig. 5f) coupled to a strong OMZ. This setting suggests stronger modification in the atmospheric regime of terrigenous fluvial input when the ITCZ-SPSH is at its northernmost position (Fig. 4b). This hypothesis is supported by other studies on the continental shelf of

CPD
11, 3211–3239, 2015

Terrigeneous material supply to the Peruvian central continental shelf

F. Briceño Zuluaga et al.

Peru (Salvatteci et al., 2014) and also in the Eastern Andes where an increase in rainfall (between ∼ 10–20 %) was detected during the LIA, with respect to the subsequent 200 years (Reuter et al., 2009). This trend is consistent with the increase in upwelling productivity (Gutiérrez et al., 2011; Salvatteci et al., 2014; Sifeddine et al., 2008) and confirms the relationship between the intensification of the upwelling activity induced by the variability of the regional winds from SPSH displacement.

The increase in the wind intensity over the past two centuries likely represents the result of the modern position of the ITCZ–SPSH system and the associated intensification of the local and regional winds (Fig. 4f). Nevertheless, the aeolian deposition material (Fig. 3f) and in consequence the wind intensity and variability of the last 100 yr are stronger than the second sequence of the MCA (Fig. 4f) under similar conditions (i.e., position of the ITZC-SPSH, Fig. 4b). This trend suggests an additional forcing in the intensification of the atmospheric circulation consistent with the pattern of climate change (England et al., 2014; Sydeman et al., 2014). Finally, the decrease in runoff in the same period displayed by the M2 component reflects a tendency for drier regional conditions in comparison with the LIA period (Fig. 4e). However, during the CWP, the wind intensification showed a close relation with the OMZ variability (Fig. 4c and f), reinforcing the interpretation of wind intensification combined with a strengthening of the SPSH.

Variations of the fluvial input exhibited a centennial pattern along the last millennium, showing intense fluvial input during the first period of the MCA and LIA. Thus, a mean climate state period of wet conditions and reduced aeolian wind intensity in this time is indicated (Fig. 4e). In contrast, little fluvial input and more vigorous wind intensity are exhibited during the second period of MCA and CWP. A good match between the Ti content record from Cariaco basin (Fig. 4b) and the decadal and centennial variation in the fluvial input in the Peruvian continental shelf supports the hypothesis that both systems are controlled by a common climatic mechanism. This condition is related to the ITCZ displacement described by Haug et al. (2001), Hyeong et al. (2006), Peterson and Haug (2006), and most recently by Sachs et al. (2009). Consequently, a displacement

CPD
11, 3211–3239, 2015

and reduction of the strength of the SPSH system over the East Pacific would be expected. Based on these trends, the three components exhibit high variability at decadal timescales of wind intensity and sediment discharge, which could be associated with El Nino-like conditions.

4 Conclusions

Four types of terrigenous components (M2, M3 and M4) related to different transport modes in the continental shelf along the last millennium were identified in a sediment record. The M2 mode is an indicator of hemipelagic fluvial input; meanwhile, the M3 and M4 components are related to aeolian transport. A vigorous transport of aeolian and fluvial components exhibits centennial variability and shows a relationship with atmospheric conditions. The MCA and CWP periods showed an increment in the wind intensity, whereas the LIA was characterized by intense fluvial input. Comparison between records reveals a coherent match between the meridional displacement of the ITCZ-SPSH system and the regional fluvial and aeolian terrigenous input variability. The aeolian input intensity and the anoxic conditions recorded by marine sediments showed a close link that suggests a mechanism associated with SPSH displacement. Changes in sediment discharge to the continental shelf are linked to the southward displacement of the ITCZ-SPSH. A progressive intensification of the wind intensity recorded during the CWP can be related to the strength of the Walker circulation, favoring La Niña events, which allow for an increase in regional wind intensity and consequently OMZ intensification. Based on this trend, our record shows high decadal variability of terrigenous vs. aeolian transport.

The Supplement related to this article is available online at doi:10.5194/cpd-11-3211-2015-supplement.

CPD
11, 3211–3239, 2015

Acknowledgements. This work was supported by the International Joint Laboratory "PALEO-TRACES" (IRD-France, UPMC-France, UFF-Brazil, UA-Chile, UPCH-Peru), the Department of Geochemistry of the Universidade Federal Fluminense-UFF (Brazil), the ALYSES analytical platform (IRD/UPMC), the Peruvian Marine Research Institute (IMARPE) and the Geophysical Peruvian Institute (IGP). It was also supported by the collaborative project Chaire Croisée PRO-SUR (IRD). We deeply thank the CAPES-Brazil for the scholarship. We are also grateful to the anonymous reviewers for their constructive and helpful suggestions to improve this manuscript.

References

Agnihotri, R., Altabet, M. A., Herbert, T. D., and Tierney, J. E.: Subdecadally resolved paleoceanography of the Peru margin during the last two millennia, Geochem. Geophys. Geosy., 9, Q05013, doi:10.1029/2007GC001744, 2008.

Alfaro, S. C., Flores-Aqueveque, V., Foret, G., Caquineau, S., Vargas, G., and Rutllant, J. A.: A simple model accounting for the uptake, transport, and deposition of wind-eroded mineral particles in the hyperarid coastal Atacama Desert of northern Chile, Earth Surf. Proc. Land., 36, 923–932, doi:10.1002/esp.2122, 2011.

Apaéstegui, J., Cruz, F. W., Sifeddine, A., Vuille, M., Espinoza, J. C., Guyot, J. L., Khodri, M., Strikis, N., Santos, R. V., Cheng, H., Edwards, L., Carvalho, E., and Santini, W.: Hydroclimate variability of the northwestern Amazon Basin near the Andean foothills of Peru related to the South American Monsoon System during the last 1600 years, Clim. Past, 10, 1967–1981, doi:10.5194/cp-10-1967-2014, 2014.

Bekaddour, T., Schlunegger, F., Vogel, H., Delunel, R., Norton, K. P., Akçar, N., and Kubik, P.: Paleo erosion rates and climate shifts recorded by Quaternary cut-and-fill sequences in the Pisco valley, central Peru, Earth Planet. Sc. Lett., 390, 103–115, doi:10.1016/j.epsl.2013.12.048, 2014.

Bloemsma, M. R., Zabel, M., Stuut, J. B. W., Tjallingii, R., Collins, J. A., and Weltje, G. J.: Modelling the joint variability of grain size and chemical composition in sediments, Sediment. Geol., 280, 135–148, doi:10.1016/j.sedgeo.2012.04.009, 2012.

Böning, P. and Brumsack, H.: Geochemistry of Peruvian near-surface sediments, Geochim. Cosmochim. Ac., 68, 4429–4451, doi:10.1016/j.gca.2004.04.027, 2004.

Ehlert, C., Grasse, P., Gutiérrez, D., Salvatteci, R., and Frank, M.: Nutrient utilisation and weathering inputs in the Peruvian upwelling region since the Little Ice Age, Clim. Past, 11, 187–202, doi:10.5194/cp-11-187-2015, 2015.

England, M. H., McGregor, S., Spence, P., Meehl, G. A., Timmermann, A., Cai, W., Gupta, A. S., McPhaden, M. J., Purich, A., and Santoso, A.: Recent intensification of wind-driven circulation in the Pacific and the ongoing warming hiatus, Nature Climate Change, 4, 222–227, doi:10.1038/nclimate2106, 2014.

Escobar Baccaro, D. F.: Evaluacion climatologica y sinoptica del fenómeno de vientos Paracas, Universidad Nacional Agraria La Molina, Lima, Peru, 1993.

Flores-Aqueveque, V., Alfaro, S. C., Caquineau, S., Foret, G., Vargas, G., and Rutllant, J. A.: Inter-annual variability of southerly winds in a coastal area of the Atacama Desert: implications for the export of aeolian sediments to the adjacent marine environment, Sedimentology, 59, 990–1000, doi:10.1111/j.1365-3091.2011.01288.x, 2012.

Flores-Aqueveque, V., Alfaro, S., Vargas, G., Rutllant, J. A., and Caquineau, S.: Aeolian particles in marine cores as a tool for quantitative high-resolution reconstruction of upwelling favorable winds along coastal Atacama Desert, Northern Chile, Prog. Oceanogr., 134, 244–255, doi:10.1016/j.pocean.2015.02.003, 2015.

Garreaud, R. and Falvey, M.: The coastal winds off western subtropical South America in future climate scenarios, Int. J. Climatol., 2, 29, 543–554, doi:10.1002/joc.1716, 2009.

Gay, S. P.: Blowing sand and surface winds in the Pisco to Chala Area, Southern Peru, J. Arid Environ., 61, 101–117, doi:10.1016/j.jaridenv.2004.07.012, 2005.

Gomes, L., Bergametti, G., Dulac, F., and Ezat, U.: Assessing the actual size distribution of atmospheric aerosols collected with a cascade impactor, J. Aerosol Sci., 21, 47–59, doi:10.1016/0021-8502(90)90022-P, 1990.

Gutiérrez, D., Sifeddine, A., Field, D. B., Ortlieb, L., Vargas, G., Chávez, F. P., Velazco, F., Ferreira, V., Tapia, P., Salvatteci, R., Boucher, H., Morales, M. C., Valdés, J., Reyss, J.-L., Campusano, A., Boussafir, M., Mandeng-Yogo, M., García, M., and Baumgartner, T.: Rapid reorganization in ocean biogeochemistry off Peru towards the end of the Little Ice Age, Biogeosciences, 6, 835–848, doi:10.5194/bg-6-835-2009, 2009.

Gutiérrez, D., Bouloubassi, I., Sifeddine, A., Purca, S., Goubanova, K., Graco, M., Field, D., Méjanelle, L., Velazco, F., Lorre, A., Salvatteci, R., Quispe, D., Vargas, G., Dewitte, B., and Ortlieb, L.: Coastal cooling and increased productivity in the main upwelling zone off Peru since the mid-twentieth century, Geophys. Res. Lett., 38, 1–6, doi:10.1029/2010GL046324, 2011.

Haug, G. H., Hughen, K. A., Sigman, D. M., Peterson, L. C., and Röhl, U.: Southward migration of the intertropical convergence zone through the Holocene, Science, 293, 1304–1308 doi:10.1126/science.1059725, 2001.

Hesse, P. P. and McTainsh, G. H.: Last Glacial Maximum to Early Holocene Wind Strength in the Mid-latitudes of the Southern Hemisphere from Aeolian Dust in the Tasman Sea, Quaternary Res., 52, 343–349, doi:10.1006/qres.1999.2084, 1999.

Holz, C., Stuut, J. B. W., Henrich, R., and Meggers, H.: Variability in terrigenous sedimentation processes off northwest Africa and its relation to climate changes: inferences from grain-size distributions of a Holocene marine sediment record, Sediment. Geol., 202, 499–508, doi:10.1016/j.sedgeo.2007.03.015, 2007.

Huang, X., Oberhänsli, H., von Suchodoletz, H., and Sorrel, P.: Dust deposition in the Aral Sea: implications for changes in atmospheric circulation in central Asia during the past 2000 years, Quaternary Sci. Rev., 30, 3661–3674, doi:10.1016/j.quascirev.2011.09.011, 2011.

Hyeong, K., Yoo, C. M., Kim, J., Chi, S.-B., and Kim, K.-H.: Flux and grain size variation of eolian dust as a proxy tool for the paleo-position of the Intertropical Convergence Zone in the northeast Pacific, Palaeogeogr. Palaeocl, 241, 214–223, doi:10.1016/j.palaeo.2006.03.011, 2006.

Iversen, J. D. and White, B. R.: Saltation threshold on Earth, Mars and Venus, Sedimentology, 29, 111–119, doi:10.1111/j.1365-3091.1982.tb01713.x, 1982.

Koopmann, B.: Sedimentation von Saharastaub im subtropischen Nordatlantik während der letzten 25.000 Jahre, Meteor. Forschungsergebnisse, 35, 23–59, 1981

Lavado Casimiro, W. S., Ronchail, J., Labat, D., Espinoza, J. C., and Guyot, J. L.: Basin-scale analysis of rainfall and runoff in Peru (1969–2004): Pacific, Titicaca and Amazonas drainages, Hydrolog. Sci. J., 57, 625–642, doi:10.1080/02626667.2012.672985, 2012.

Mann, M., Zhang, Z., and Rutherford, S.: Global signatures and dynamical origins of the Little Ice Age and Medieval Climate Anomaly, Science, 326, 1256–1260, doi:10.1126/science.1177303, 2009.

Martincorena.: Dust productions mechanism, in: Mineral Dust: A Key Player in the Earth System, edited by: Knippertz, P. and Stuut, J.-B., Springer, Dordrecht, Heidelberg, New York, London, 90–120, 2014.

Marticorena, B. and Bergametti, G.: Modeling the atmospheric dust cycle: 1. Design of a soil-derived dust emission scheme, J. Geophys. Res., 100, 16415, doi:10.1029/95JD00690, 1995.

McCave, I. N., Manighetti, B., and Robinson, S. G.: Sortable silt and fine sediment size/composition slicing: parameters for palaeocurrent speed and palaeoceanography, Paleoceanography, 10, 593–610, 1995.

McTainsh, G. H., Nickling, W. G., and Lynch, A. W.: Dust deposition and particle size in Mali, West Africa, Catena, 29, 307–322, doi:10.1016/S0341-8162(96)00075-6, 1997.

Meyer, I., Davies, G. R., and Stuut, J. B. W.: Grain size control on Sr-Nd isotope provenance studies and impact on paleoclimate reconstructions: an example from deep-sea sediments offshore NW Africa, Geochem. Geophys. Geosy., 12, 14, doi:10.1029/2010GC003355, 2011.

Molina-Cruz, A.: The relation of the southern trade winds to upwelling processes during the last 75,000 years, Quaternary Res., 8, 324–338, doi:10.1016/0033-5894(77)90075-8, 1977.

Montes, I., Colas, F., Capet, X., and Schneider, W.: On the pathways of the equatorial subsurface currents in the eastern equatorial Pacific and their contributions to the Peru-Chile Undercurrent, J. Geophys. Res., 115, C09003, doi:10.1029/2009JC005710, 2010.

Oppo, D. W., Rosenthal, Y., and Linsley, B. K.: 2,000-year-long temperature and hydrology reconstructions from the Indo-Pacific warm pool, Nature, 460, 1113–1116, doi:10.1038/nature08233, 2009.

Ortlieb, L.: The documented historical record of El Nino events in Peru: an update of the Quinn record (sixteenth throught nineteenth centuries), in: El Nino and the Southern Oscillation, Multiscale Variability and Global and Regional Impacts, Cambridge University Press, UK, 207–295, 2000.

Parkin, D. W. and Shackleton, N..: Trade wind and temperature correlations down a deep sea core off the Sharan coast, Nature, 245, 455–457, 1973.

Peterson, L. and Haug, G.: Variability in the mean latitude of the Atlantic Intertropical Convergence Zone as recorded by riverine input of sediments to the Cariaco Basin (Venezuela), Palaeogeogr. Palaeocl., 234, 97–113, doi:10.1016/j.palaeo.2005.10.021, 2006.

Pichevin, L., Cremer, M., Giraudeau, J., and Bertrand, P.: A 190 ky record of lithogenic grain-size on the Namibian slope: forging a tight link between past wind-strength and coastal upwelling dynamics, Mar. Geol., 218, 81–96, doi:10.1016/j.margeo.2005.04.003, 2005.

Prins, M.: Pelagic, hemipelagic and turbidite deposition in the Arabian Sea during the late Quaternary, Utrecht, Utrecht University, Geologica Ultraiectina, 168, 192 pp., 1999.

Prins, M. A., Vriend, M., Nugteren, G., Vandenberghe, J., Lu, H., Zheng, H., and Jan Weltje, G.: Late Quaternary aeolian dust input variability on the Chinese Loess Plateau: inferences from unmixing of loess grain-size records, Quaternary Sci. Rev., 26, 230–242, doi:10.1016/j.quascirev.2006.07.002, 2007.

Quijano Vargas, J. J.: Estudio numerico y observacional de la frente a la costa de Ica-Perú, Lima, Perú, 2013.

Ratmeyer, V., Fischer, G., and Wefer, G.: Lithogenic particle fluxes and grain size distributions in the deep ocean off northwest Africa: implications for seasonal changes of aeolian dust input and downward transport, Deep-Sea Res. Pt. I, 46, 1289–1337, 1999.

Rein, B.: El Niño variability off Peru during the last 20,000 years, Paleoceanography, 20, PA4003, doi:10.1029/2004PA001099, 2005.

Rein, B.: How do the 1982/83 and 1997/98 El Niños rank in a geological record from Peru?, Quatern. Int., 161, 56–66, doi:10.1016/j.quaint.2006.10.023, 2007.

Rein, B., Lückge, A., and Sirocko, F.: A major Holocene ENSO anomaly during the Medieval period, Geophys. Res. Lett., 31, L17211, doi:10.1029/2004GL020161, 2004.

Reuter, J., Stott, L., Khider, D., Sinha, A., Cheng, H., and Edwards, R. L.: A new perspective on the hydroclimate variability in northern South America during the Little Ice Age, Geophys. Res. Lett., 36, L21706, doi:10.1029/2009GL041051, 2009.

Sachs, J. P., Sachse, D., Smittenberg, R. H., Zhang, Z., Battisti, D. S., and Golubic, S.: Southward movement of the Pacific intertropical convergence zone AD 1400–1850, Nat. Geosci., 2, 519–525, doi:10.1038/ngeo554, 2009.

Wang, J., Emile-Geay, J., Guillot, D., Smerdon, J. E., and Rajaratnam, B.: Evaluating climate field reconstruction techniques using improved emulations of real-world conditions, Clim. Past, 10, 1–19, doi:10.5194/cp-10-1-2014, 2014.

Saukel, C., Lamy, F., Stuut, J. B. W., Tiedemann, R., and Vogt, C.: Distribution and provenance of wind-blown SE Pacific surface sediments, Mar. Geol., 280, 130–142, doi:10.1016/j.margeo.2010.12.006, 2011.

Scheidegger, K. F. and Krissek, L. A.: Dispersal and deposition of eolian and fluvial sediments off Peru and northern Chile, Geol. Soc. Am. Bull., 93, 150–162, doi:10.1130/0016-7606(1982)93<150:DADOEA>2.0.CO;2, 1982.

CPD

11, 3211–3239, 2015

Terrigeneous material supply to the Peruvian central continental shelf

F. Briceño Zuluaga et al.

Schweigger, E.: El litoral Peruano, 2nd edn., Universidad Nacional Federico Villareal, Lima 4141964 pp., 164.
Sears, M.: Notes on the Peruvian coastal current. 1. An introduction to the ecology of Pisco Bay, Deep-Sea Res., 1, 141–169, doi:10.1016/0146-6313(54)90045-3, 1954.
Shao, Y. and Lu, H.: A simple expression for wind erosion threshold friction velocity, J. Geophys. Res., 105, 22437, doi:10.1029/2000JD900304, 2000.
Shao, Y., Ishizuka, M., Mikami, M., and Leys, J. F.: Parameterization of size-resolved dust emission and validation with measurements, J. Geophys. Res.-Atmos., 116, 1–19, doi:10.1029/2010JD014527, 2011.
Sifeddine, A., Gutiérrez, D., Ortlieb, L., Boucher, H., Velazco, F., Field, D., Vargas, G., Boussafir, M., Salvatteci, R., Ferreira, V., García, M., Valdés, J., Caquineau, S., Mandeng Yogo, M., Cetin, F., Solis, J., Soler, P., and Baumgartner, T.: Laminated sediments from the central Peruvian continental slope: a 500 year record of upwelling system productivity, terrestrial runoff and redox conditions, Prog. Oceanogr., 79, 190–197, doi:10.1016/j.pocean.2008.10.024, 2008.
Stuut, J. W., Prins, M. A., and Weltje, G. J.: The palaeoclimatic record provided by aeolian dust in the deep sea: proxies and problems, Geophys. Res. Abstr., 7, 10886, doi:1607-7962/gra/EGU05-A-10886, 2005.
Stuut, J.-B. W., Kasten, S., Lamy, F., and Hebbeln, D.: Sources and modes of terrigenous sediment input to the Chilean continental slope, Quatern. Int., 161, 67–76, doi:10.1016/j.quaint.2006.10.041, 2007.
Stuut, J.-B. W., and Lamy, F.: Climate variability at the southern boundaries of the Namib (southwestern Africa) and Atacama (northern Chile) coastal deserts during the last 120,000 yr, Quaternary Res., 62, 301–309, doi:10.1016/j.yqres.2004.08.001, 2004.
Stuut, J.-B. W., Prins, M. A., Schneider, R. R., Weltje, G. J., Jansen, J. H. F., and Postma, G.: A 300-kyr record of aridity and wind strength in southwestern Africa: inferences from grain-size distributions of sediments on Walvis Ridge, SE Atlantic, Mar. Geol., 180, 221–233, doi:10.1016/S0025-3227(01)00215-8, 2002.
Sun, D., Bloemendal, J., Rea, D., Vandenberghe, J., Jiang, F., An, Z., and Su, R.: Grain-size distribution function of polymodal sediments in hydraulic and aeolian environments, and numerical partitioning of the sedimentary components, Sediment. Geol., 152, 263–277, doi:10.1016/S0037-0738(02)00082-9, 2002.

Sydeman, W. J., García-Reyes, M., Schoeman, D. S., Rykaczewski, R. R., Thompson, S. A., Black, B. A., and Bograd, S. J.: Climate change and wind intensification in coastal upwelling ecosystems, Science, 345, 77–80, doi:10.1126/science.1251635, 2014.

Unkel, I., Kadereit, A., Mächtle, B., Eitel, B., Kromer, B., Wagner, G., and Wacker, L.: Dating methods and geomorphic evidence of palaeoenvironmental changes at the eastern margin of the South Peruvian coastal desert (14°30′ S) before and during the Little Ice Age, Quatern. Int., 175, 3–28, doi:10.1016/j.quaint.2007.03.006, 2007.

Weltje, G. J.: End-member modeling of compositional data: numerical-statistical algorithms for solving the explicit mixing problem, Math. Geol., 29, 503–549, doi:10.1007/BF02775085, 1997.

Weltje, G. and Prins, M.: Sources and dispersal patterns of deep-marine siliciclastics: inferences from end-member modeling of grain-size distributions, Proc. 2001 Annu. Conf., Cancun, Mexico, 1–10, 2001.

Weltje, G. J. and Prins, M. A.: Muddled or mixed? Inferring palaeoclimate from size distributions of deep-sea clastics, Sediment. Geol., 162, 39–62, doi:10.1016/S0037-0738(03)00235-5, 2003.

Weltje, G. J. and Prins, M. A.: Genetically meaningful decomposition of grain-size distributions, Sediment. Geol., 202, 409–424, doi:10.1016/j.sedgeo.2007.03.007, 2007.

Wentworth, C. K.: A Scale of Grade and Class Terms for Clastic Sediments, J. Geol., 30, 377–392, doi:10.1086/622910, 1922.

CPD
11, 3211–3239, 2015

CPD
11, 3211–3239, 2015

Terrigeneous material supply to the Peruvian central continental shelf

F. Briceño Zuluaga et al.

Title Page
Abstract | Introduction
Conclusions | References
Tables | Figures
Back | Close
Full Screen / Esc
Printer-friendly Version
Interactive Discussion

Table 1. Minimum, maximum and average values to the grain size components in each unit obtained along the record in the Pisco continental shelf.

	First period MCA 900–1170 AD		Second period MCA 1170–1450 AD		LIA 1450–1800 AD		CWP 1900 to present	
Grain size componens	$dV/d\ln d$ (%)		$dV/d\ln d$ (%)		$dV/d\ln d$ (%)		$dV/d\ln d$ (%)	
	Av/SD	Range (Min.–Max.)	Av/SD	Range (Min.–Max.)	Av/SD	Range (Min.–Max.)	Av/SD	Range (Min.–Max.)
M1	11 ± 4	7–19	14 ± 6,0	5–27	15 ± 6	6–28	18 ± 7	4–40
M2	50 ± 10	33–64	41 ± 10	23–62	57 ± 13	25–80	34 ± 10	13–63
M3	18 ± 7	6–28	21 ± 9	0–39	16 ± 8	5–45	23 ± 10	6–44
M4	21 ± 8	8–42	24 ± 15	0–55	11 ± 7	0–24	25 ± 13	0–56

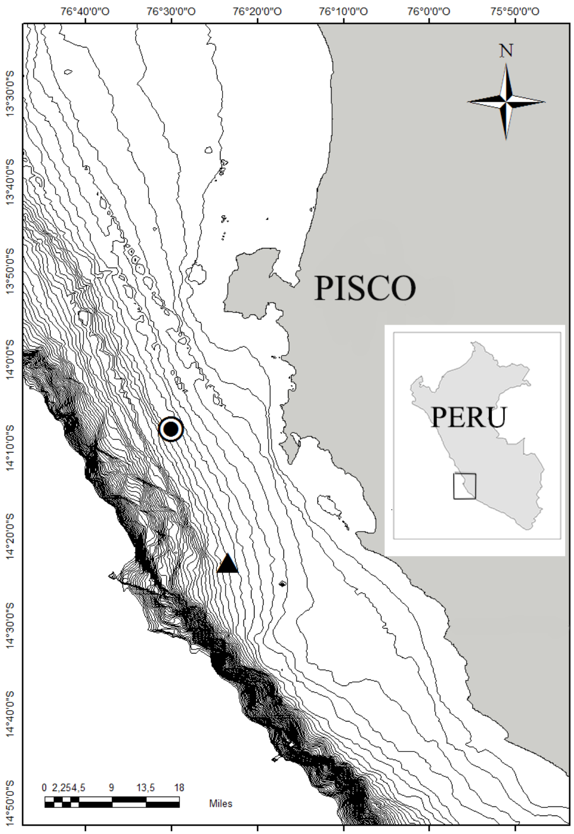

Figure 1. Location of the sampling of the sediment cores B040506 (black circle) and G10-GC-01(black triangle) in the Central Peru continental margin.

CPD
11, 3211–3239, 2015

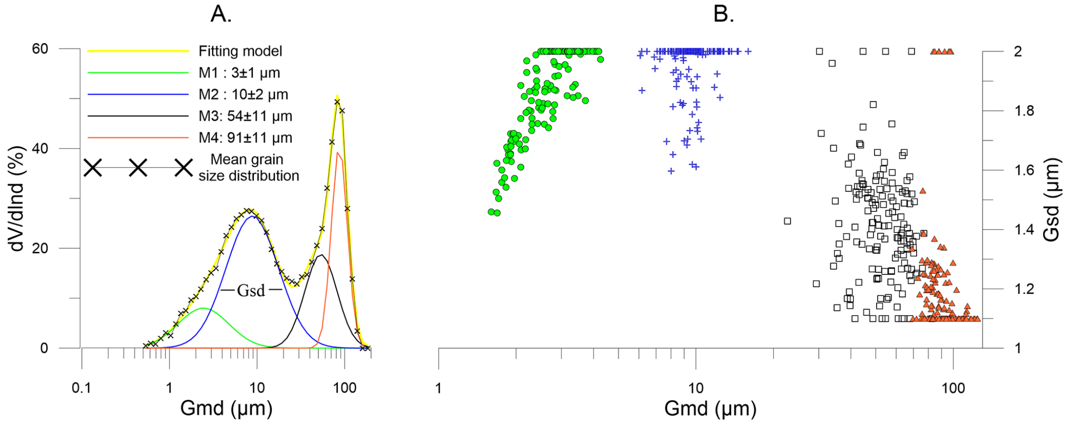

Figure 2. (a) Description of the four modes fitted calculates (M1, M2, M3 and M4) for the mean grain size of the total record; in detail is showed an example of geometrical standard deviation (Gsd) and its frequency (dV/dlnd(%)) and **(b)** the Gsd and geometrical mean diameter (Gmd) plotted of the unmixed components.

CPD
11, 3211–3239, 2015

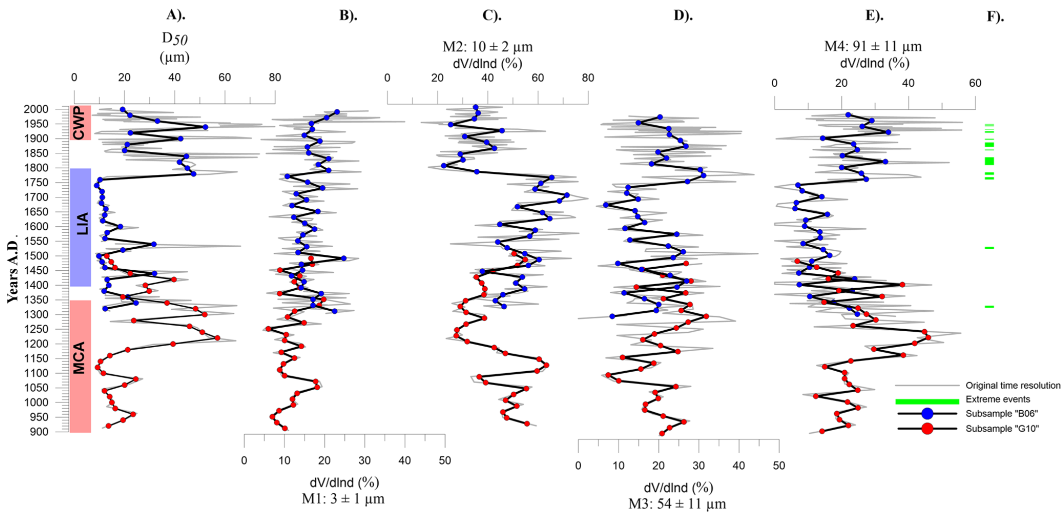

Figure 3. (a) The median grain size (D50) variation along the record and variation in relative abundance of the sedimentary components: **(b)** M1, **(c)** Fluvial (M2), **(d)** Aeolian (M3) and **(e)** Aeolian (M4) of the grain size distribution in the record **(f)** Represent the samples where was found very large particles related with extreme events.

CPD
11, 3211–3239, 2015

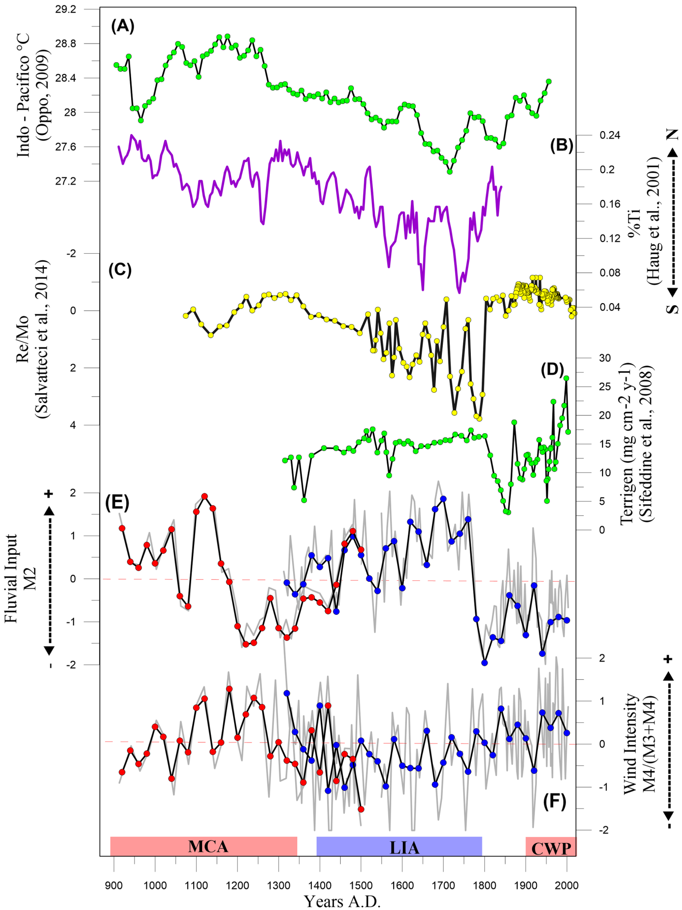

CPD
11, 3211–3239, 2015

Terrigeneous material supply to the Peruvian central continental shelf

F. Briceño Zuluaga et al.

Figure 4. Reconstruction of **(a)** Indo-Pacific temperatures reconstruction (Oppo et al., 2009), **(b)** ITCZ migration (%Ti) (Peterson and Haug, 2006), **(c)** OMZ activity (Re/Mo anomalies) (Salvatteci et al., 2014), **(d)** terrigenous flux in Pisco continental shelf by Sifeddine et al. (2008), **(e)** fluvial input (M2) anomaly reconstruction on the continental shelf, **(f)** wind intensity (M4/(M3 + M4)) anomaly reconstruction.

CPD

11, 3211–3239, 2015

Terrigeneous material supply to the Peruvian central continental shelf

F. Briceño Zuluaga et al.